A Net Sink for Atmospheric CH_3Br in the East Pacific Ocean

Jürgen M. Lobert, James H. Butler, Stephen A. Montzka, Laurie S. Geller, Richard C. Myers, James W. Elkins

Surface waters along a cruise track in the East Pacific Ocean were undersaturated in methyl bromide (CH_3Br) in most areas except for coastal and upwelling regions, with saturation anomalies ranging from +100 percent in coastal waters to −50 percent in open ocean areas, representing a regionally weighted mean of −16 (−13 to −20) percent. The partial lifetime of atmospheric CH_3Br with respect to calculated oceanic degradation along this cruise track is 3.0 (2.9 to 3.6) years. The global, mean dry mole fraction of CH_3Br in the atmosphere was 9.8 ± 0.6 parts per trillion, with an interhemispheric ratio of 1.31 ± 0.08. These data indicate that ~8 percent (0.2 parts per trillion) of the observed interhemispheric difference in atmospheric CH_3Br could be attributed to an uneven global distribution of oceanic sources and sinks.

Methyl bromide (CH_3Br) has received considerable attention recently (*1–11*), in particular because of its high ozone depletion potential (*5, 6*). The tropospheric mixing ratio of organic bromine is believed to be ~20 parts per trillion (ppt), to which CH_3Br contributes ~50% (*5, 7*). However, the atmospheric CH_3Br budget is uncertain at this time, particularly with regard to oceanic contributions (*1, 2, 3, 10*).

Annual fluxes of CH_3Br to the atmosphere could range from 76 to 198 Gg (1 Gg = 10^9 g), based on reported atmospheric mixing ratios (*2*) and lifetimes (*12, 13*). Emissions from industrial activities (2 to 10%), soil fumigation (20 to 60%), and biomass burning (10 to 50%) have been estimated to contribute 33 to 74% to the total flux of CH_3Br to the atmosphere (*5, 8, 9*); the remainder of global emissions has historically been attributed to the oceans. Singh *et al.* (*10*) found saturation anomalies of 180 to 240% for the East Pacific Ocean, and Khalil *et al.* (*3*) found saturation anomalies of 40 to 80% for the Pacific Ocean. The reasons for the discrepancy between these results are unknown, but it could be caused by sampling and analytical differences or by geographic differences in the distribution of dissolved CH_3Br. Singh *et al.* (*10*) measured CH_3Br mainly in productive nearshore waters and areas close to the upwelling regions of the Americas, whereas Khalil *et al.* (*3*) derived their estimate mainly from the open ocean. Singh *et al.* compared in situ atmospheric partial pressures with surface water concentrations, which required solubility data to obtain saturation anomalies, whereas Khalil *et al.* collected air in stainless steel flasks and directly compared partial pressures of CH_3Br in the atmosphere with those above equilibrated surface water.

For the National Oceanic and Atmospheric Administration (NOAA)–Climate Monitoring and Diagnostics Laboratory Bromine Latitudinal Air-Sea Transect 1994 (BLAST 94) expedition, a transit leg of the World Ocean Circulation Experiment Line P18 was selected because it covered coastal waters, central oceanic gyres, and regions of divergence and upwelling in both hemispheres, as well as two different seasons. We made measurements aboard ship to eliminate artifacts associated with storage of samples, and partial pressures were measured directly to remove the dependence of saturation anomalies on currently uncertain solubility data. A mass spectrometer (MS) was selected over an electron capture detector (ECD) for measurement of CH_3Br to circumvent potential interferences common to the use of ECDs.

Research was conducted aboard the *NOAA Ship Discoverer* between 26 January and 18 February 1994. The 13,600-km cruise track led from 48°N to 54°S in the East Pacific Ocean (Fig. 1). Ambient air was sampled at the most forward point of the ship, ~15 m above the ocean surface. For the partitioning of gases in surface seawater, we used an acrylic equilibrator (*14, 15*). The approximate residence time of air and equilibrator headspace in the sampling setup was ~1 min, and the average sample spacing was ~30 km (one sample per hour). Instrumental precision (1 σ) for CH_3Br was better than 2%; the detection limit (3 σ) was <0.5 ppt of CH_3Br (*16*). Measurements were standardized with frequent injections of natural air, calibrated with gravimetric standards prepared in our laboratory.

Several tests were conducted at sea to ensure that the data were not marred by analytical or sampling artifacts. Although CH_3Br was usually detected as $[CH_3{}^{81}Br]^+$ (mass to charge ratio $m/z^+ = 96$), it occasionally was monitored as $[CH_3{}^{79}Br]^+$ ($m/z^+ = 94$) to ensure that mass fractionation or an interference by other compounds was not affecting the results. No peaks with ion 94 or 96 eluted near CH_3Br. No blank signals were detected when purified halocarbon-free air was periodically injected. Finally, the equilibrator was tested for potential internal loss or production of analyte gases, and an alternative sampling scheme, which allowed for sampling without any devices other than valves in the sample stream, was used on occasion. All of these tests showed no analytical or sampling interferences that would significantly affect the determination of CH_3Br saturation anomalies.

Flasks of ambient air and equilibrator headspace were filled every few degrees of latitude. All flasks were analyzed with separate gas chromatography–mass spectroscopy (GC-MS) and GC-ECD instruments over a period of several months after the cruise. Most of those results agreed with shipboard data, although some flasks

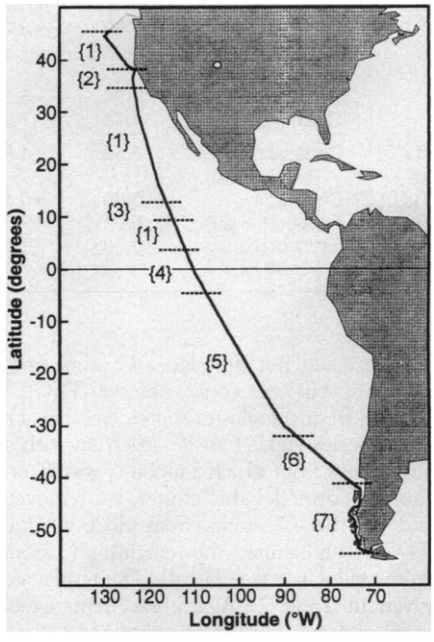

Fig. 1. Cruise track of the *NOAA Ship Discoverer*, January–February 1994. Horizontal dashed lines indicate oceanic regions used for the computation of results: region 1, open ocean (winter); region 2, coastal waters (winter); region 3, divergence between the North Equatorial Current and the North Equatorial Countercurrent; region 4, equatorial divergence (upwelling); region 5, open ocean (summer); region 6, coastal and nearshore waters (summer); and region 7, inland passage.

J. M. Lobert and L. S. Geller, National Oceanic and Atmospheric Administration, Climate Monitoring and Diagnostics Laboratory, 325 Broadway, Boulder, CO 80303, USA, and Cooperative Institute for Research in Environmental Sciences, University of Colorado, Boulder, CO 80309, USA.
J. H. Butler, S. A. Montzka, R. C. Myers, J. W. Elkins, National Oceanic and Atmospheric Administration, Climate Monitoring and Diagnostics Laboratory, 325 Broadway, Boulder, CO 80303, USA.

showed significant differences owing to storage effects. We confirmed the undersaturations determined by the two GC-MS systems with a GC-ECD system equipped with a Poraplot Q column. The results of a GC-ECD analysis made with a DB-1 column, however, disagreed and, in fact, showed supersaturations where there were undersaturations according to three other analytical systems.

The smoothed atmospheric mole fraction obtained from shipboard measurements of CH_3Br ranged from 10 to 12 ppt in the mid- to high latitudes of the Northern Hemisphere (NH) to 7 to 9 ppt in the higher latitudes of the Southern Hemisphere (SH) (Fig. 2A), with mean hemispheric mole fractions of 11.1 ± 0.6 ppt (NH) and 8.5 ± 0.6 ppt (SH) (*17*). The global mean mole fraction of CH_3Br was 9.8 ± 0.6 ppt. Whether the break between hemispheres was selected at the equator (0°) or at the interhemispheric tropical convergence zone (ITCZ; 5°N), the ratio of total CH_3Br between hemispheres (NH/SH) remained at 1.31 (*18*).

The partial pressure profile of surface water (Fig. 2B) differs distinctly from the atmospheric profile and even more so from data reported by other investigators (*3*, *10*). The partial pressure of CH_3Br in the surface water was generally lower than that in the atmosphere. Moreover, dissolved CH_3Br did not correlate with dissolved CH_3Cl or CH_3I at a 90% confidence level (correlation coefficient r = 0.061 and 0.196; n = 249), as has been suggested in the past (*2*, *10*); CH_3Cl and CH_3I were highly supersaturated along this cruise track and thus a correlation is not useful for directly predicting oceanic CH_3Br.

The saturation anomaly (*19*) of CH_3Br appears to be driven mainly by variations in its surface water partial pressures (Fig. 2, B and C). Moderate supersaturations were found off the coast of California and in upwelling regions at 11°N and the equator (1°S), as well as in the coastal inland passage of Chile south of 41°S. Supersaturations as high as 100% were found offshore of the coast of Chile (38°S). Most important, however, CH_3Br was undersaturated in the open ocean in both hemispheres.

To estimate the global significance of these results, we calculated mean saturation anomalies for separate physiographic areas, and our observations within each area were assumed to be representative for the entire ocean. These divisions were based on oceanic upwelling and current patterns, surface water data on nitrous oxide (*20*), and abrupt changes in the saturation anomalies of CH_3Br. Data within areas 1 to 6 (Figs. 1 and 2C) were combined into three general regions to obtain means for the open ocean, current divergences, and coastal waters (Tables 1 and 2). Saturation anomalies in the inland passage (region 7) were around +11% and varied greatly, apparently with freshwater inflow. Thus, these anomalies are probably not globally representative for any large area of the ocean and were disregarded in flux computations.

The global mean net saturation anomaly, derived from weighting the three general regions according to their presumed oceanic coverage, was −15.7% (−13 to −20%) (Table 2) (*21*). One departure from general undersaturation in open ocean areas was observed as the ship passed the Humboldt Current (30° to 35°S), a feature that was included in the estimate for coastal waters. Were this feature considered as part of the open ocean, the global net saturation anomaly would become −13%. Similarly, if the inland passage were included as part of the coastal region, the mean net anomaly would become −17%.

Although the data presented here were collected along a cruise track selected for its coverage of major oceanographic regions during austral summer and boreal winter, they still represent only the East Pacific Ocean. Hence, these averages might be limited in their ability to represent global oceanic regimes. However, until larger areas of the ocean are explored, these are the best estimates we can currently derive.

The flux of CH_3Br across the air-sea interface, corrected for physical effects (*19*), should equal the sum of in situ loss and production in surface waters. If we assume that the saturation anomaly of CFC-11 ($\Delta_{CFC\text{-}11}$) is adequate in correcting for these effects, then, under steady-state conditions,

Table 1. Observed values for CH_3Br in three main marine regions. SST, average sea-surface temperature as measured during the cruise; V, average true wind speed as observed during the cruise; mean Δ_{CH_3Br}, saturation anomaly of CH_3Br (*19*); mean $\Delta_{CFC\text{-}11}$, saturation anomaly of CFC-11 (chlorofluorocarbon-11) (*19*).

Region	SST (°C)	V (m s^{-1})	Δ_{CH_3Br} (%)	$\Delta_{CFC\text{-}11}$ (%)
Open ocean {1, 5}	21.9	7.1	−21.8	2.5
Coastal {2, 6}	17.6	7.2	40.3	2.9
Upwelling {3, 4}	26.1	6.3	1.4	0.6

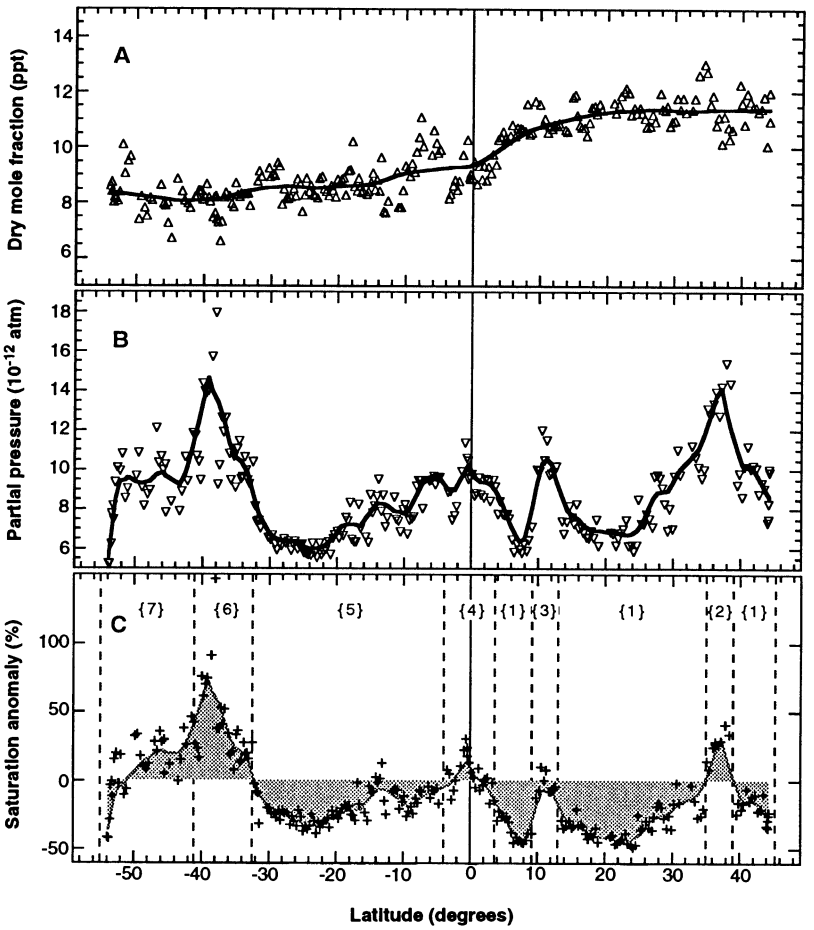

Fig. 2. Data on CH_3Br in the air and water of the East Pacific Ocean. (**A**) Dry mole fraction of atmospheric CH_3Br, (**B**) its partial pressure in the surface water, and (**C**) the saturation anomaly (shaded area) and net saturation anomaly (line and markers). Solid lines are LOESS fits (*23*); the vertical dashed lines and labels indicate the oceanic regions as described in Fig. 1.

Table 2. Calculated coefficients and fluxes for CH_3Br in three main marine regions. The weighting factor is the fraction of global ocean coverage. The open ocean was estimated to occupy 80% of all oceans, while coastal waters and upwelling regions were assumed to represent each 10% (*21*) of the global ocean area of 361×10^{12} m^2 (*24*). All results are means derived from single data points as observed during the cruise or are calculated from those. H_g, average reciprocal solubility for CH_3Br; K_w, average air-sea exchange coefficient for CH_3Br after Wanninkhof (*28*); F_{net}, net ocean-air flux (the conversion factor into gigamoles per year is 1/95) after Eq. 1; L, absolute loss (negative), the sum of nucleophilic displacement by Cl^- ions, neutral hydrolysis, and downward removal (*1, 10, 22*); P, absolute in situ production, the difference of net flux and in situ consumption. The global net saturation anomaly was derived from weighting the numbers in rows 1 to 3 with the weighting factor.

Region	Weighting factor	$\Delta_{CH_3Br} - \Delta_{CFC\text{-}11}$ (%)	H_g (m^3-atm mol^{-1})	K_w (m day^{-1})	F_{net} (Gg $year^{-1}$)	L (Gg $year^{-1}$)	P global (Gg $year^{-1}$)	P per unit area (g m^{-2} $year^{-1}$)
Open ocean {1, 5}	0.8	−24.3%	6.67×10^{-3}	4.9	−16.15	−121.8	+105.6	3.7×10^{-4}
Coastal {2, 6}	0.1	37.1%	5.64×10^{-3}	4.2	3.47	−14.5	+18.0	5.0×10^{-4}
Upwelling {3, 4}	0.1	0.65%	7.69×10^{-3}	3.9	0.04	−27.6	+27.6	7.6×10^{-4}
Global		−15.7%			−12.64	−163.9	151.2	

the net flux of CH_3Br that is required to maintain the observed net saturation anomaly (in moles per square meter per day) is given by

$$F_{net} = P - L = \frac{K_w p_a}{H_g}\left(\frac{\Delta_{CH_3Br} - \Delta_{CFC\text{-}11}}{100}\right) \quad (1)$$

where F_{net}, P, L, K_w, and H_g are defined in Table 2, p_a is the partial pressure of the gas in the atmosphere, and Δ_{CH_3Br} and $\Delta_{CFC\text{-}11}$ are saturation anomalies (in percent). Consequently, aquatic degradation exceeds aquatic production where the net saturation anomaly is negative and vice versa. The sum of the degradation rates for hydrolysis and aquatic displacement of Br in CH_3Br by Cl^- ranges from less than 1% per day in 5°C seawater to more than 30% per day in 30°C seawater and can be calculated with reasonable certainty from water temperature alone (*10, 22*). Production of CH_3Br (P), then, is estimated as the difference between net flux (F_{net}) and loss (L). This balance of production and loss in the ocean determines the saturation anomaly, hence the net emission, of CH_3Br. From data presented here, we calculate a global net flux of -12.6 ± 6.3 Gg $year^{-1}$ (Table 2).

An observed natural variability of only ±6.3% or ±0.6 ppt in atmospheric data (*23*) indicates that the interhemispheric difference of 2.6 ppt is significant at a >99% confidence level and that there is no observable influence of oceanic concentrations on the mixing ratios in the lower marine boundary layer. Also, the interhemispheric ratio is indicative of significantly greater NH emissions or SH sinks for atmospheric CH_3Br. With equally distributed global sinks, this ratio would imply that NH emissions are greater by a factor of 2.4 than SH emissions. Most of the coastal areas, where CH_3Br apparently is emitted to the atmosphere, are indeed located in the NH. However, the SH oceans cover an area 1.3 times that of NH oceans (*24*). Hence, an uneven distribution of oceanic sources and sinks may cause part of the observed atmospheric gradient. With 80% of all coastal waters located in the NH, we estimate the net flux into the SH oceans to be 1.7 times larger than that into the NH oceans. The combined effects could account for about 0.2 ppt, or 8%, of the observed interhemispheric difference, which still suggests that two-thirds of the emissions external to the oceans must emanate from the NH.

Because a net saturation anomaly results from both production and loss terms in the surface water (Eq. 1 and Table 2), the loss term must be separated from production to compute the partial lifetime of atmospheric CH_3Br with respect to the ocean (*1*). From published degradation rates for CH_3Br (*22*) and measurements of sea-surface temperature and wind speed taken during the cruise, this approach yields a partial lifetime for CH_3Br of 2.9 to 3.6 years for the three regions, with a best global estimate of 3.0 years (*25*). This value, combined with a lifetime of 1.7 to 2.1 years for the atmospheric removal by OH (*12, 13*) and stratospheric processes (*26*), yields a total lifetime of 1.16 years (1.07 to 1.33 years) for CH_3Br in the atmosphere. This lifetime estimate, along with assumptions for calculating the ozone depletion potential (ODP) as described in Mellouki *et al.* (*12*), corresponds to an ODP for CH_3Br of 0.44, which is considerably smaller than the estimate of 0.65 based on atmospheric removal of CH_3Br alone.

From the global mean mole fraction of 9.8 ppt and the lifetime of 1.7 to 2.1 years due to atmospheric processes, we calculate an annual sink of 78 to 97 Gg. Adding an amount for oceanic degradation of 46 to 57 Gg $year^{-1}$, computed from the oceanic lifetime of 2.9 to 3.6 years, yields a total sink of 124 to 154 Gg $year^{-1}$, with a best estimate, based on the combined lifetime of 1.1 year, of 142 Gg $year^{-1}$. These losses, plus 0 to 5 Gg $year^{-1}$ for growth (*3, 11*), must be balanced by all sources, including that from the oceans. Conversely, adding the observed air-to-sea flux of 6 to 19 Gg $year^{-1}$ to tropospheric and stratospheric losses leaves 84 to 116 Gg $year^{-1}$ for emissions external to the oceans, such as those due to agriculture, industrial use, and biomass burning.

Note added in proof: An expedition across the Atlantic Ocean between 53°N and 47°S at ~30°W, conducted during the review of this report, yielded results that are both qualitatively and quantitatively consistent with the findings presented here (*27*).

REFERENCES AND NOTES

1. J. H. Butler, *Geophys. Res. Lett.* **21**, 185 (1994).
2. H. Singh and M. Kanakidou, *ibid.* **20**, 133 (1993).
3. M. A. K. Khalil, R. A. Rasmussen, R. Gunawardena, *J. Geophys. Res.* **98D**, 2887 (1993).
4. C. E. Reeves and S. A. Penkett, *Geophys. Res. Lett.* **20**, 1563 (1993).
5. D. L. Albritton and R. T. Watson, in *Methyl Bromide: Its Atmospheric Science, Technology, and Economics, Montreal Protocol Assessment Supplement*, R. T. Watson, D. L. Albritton, S. O. Anderson, S. Lee-Bapty, Eds. (United Nations Environmental Programme, Nairobi, Kenya, 1992), pp. 3–18.
6. *Scientific Assessment of Ozone Depletion: 1991* (World Meteorological Organization, Geneva, 1992), p. 4.15.
7. S. M. Schauffler *et al.*, *Geophys. Res. Lett.* **20**, 2567 (1993).
8. K. Yagi, J. Williams, N.-Y. Wang, R. J. Cicerone, *Proc. Natl. Acad. Sci. U.S.A.* **90**, 8420 (1993).
9. S. Manö and M. O. Andreae, *Science* **263**, 1255 (1994).
10. H. B. Singh, L. J. Salas, R. E. Stiles, *J. Geophys. Res.* **88D**, 3684 (1983).
11. R. J. Cicerone, L. E. Heidt, W. H. Pollock, *ibid.* **93D**, 3745 (1988).
12. A. Mellouki *et al.*, *Geophys. Res. Lett.* **19**, 2059 (1992).
13. Z. Zhang *et al.*, *ibid.*, p. 2413.
14. Designed by R. F. Weiss of Scripps Institute of Oceanography [see J. H. Butler *et al.*, *NOAA Data Rep. ERL ARL-16* (NOAA, Boulder, CO, 1988)].
15. J. H. Butler, J. W. Elkins, T. M. Thompson, B. D. Hall, *J. Geophys. Res.* **96D**, 22347 (1991).
16. For shipboard measurements, ~200 ml of sample air was concentrated onto an Al_2O_3-KCl-coated, fused-silica trap (10 cm by 0.53 mm) at −50°C after passing through a P_2O_5-coated dryer (Sicapent). The trap was heated to 110°C, and the sample was injected onto a DB-5 column (30 m by 0.25 mm), which was temperature-programmed from 20° to 180°C. The column was further heated to 220°C for another 15 min to purge highly retained species. Trapping efficiency, dryer reliability, and linearity were verified on another similar instrument.
17. The hemispheric mole fraction was determined from

$$\bar{x}_{a,hem} = \frac{\sum_i x'_a \left[\frac{n_a}{2}(\sin\Theta_i - \sin\Theta_{i-1})\right]}{n_{hem}} \quad (2)$$

Here, $\bar{x}_{a,hem}$ is the hemispheric mole fraction, x_a^i are the measured atmospheric mole fractions of the compound, n_a and n_{hem} are the total number of moles in the atmosphere and hemisphere, respectively, ($n_a = 1.77 \times 10^{20}$ mol), and Θ_i and Θ_{i-1} are, respectively, the latitudes at the beginning and at the end of each incremental interval. Constant mixing ratios were assumed between 45.3° and the North Pole (11.55 ppt) and between −53.3° and the South Pole (8.25 ppt).

18. If we change the ITCZ from 0° to 5°N, the hemispheric means change from 11.1 to 11.3 ppt for the NH and from 8.5 to 8.6 ppt for the SH.
19. The saturation anomaly (in percent) is defined as the departure of the observed dissolved amount from equilibrium:

$$\Delta_g = 100\left(\frac{p_w - p_a}{p_a}\right) \quad (3)$$

where p_w and p_a are the partial pressures of the gas in water and air, respectively. Because inert compounds like CFC-11 do not react with seawater, the departures of their surface partial pressures from equilibrium are directly attributable to physical processes, such as warming and cooling, advection, or mixing, and can be used under certain conditions to factor out physical effects for gases that are not conservative in the surface ocean (*15*). In Eq. 1, a net saturation anomaly is calculated by subtracting the CFC-11 saturation anomaly from the observed anomaly of CH_3Br.
20. H. J. McLellan, *Elements of Physical Oceanography* (Pergamon, Oxford, 1965). Nitrous oxide is a strong indicator for upwelling regions and was measured during this cruise in both air and surface water with a GC-ECD system.
21. J. H. Ryther [*Science* **166**, 72 (1969)] assumed 9.9% for coastal waters including offshore areas of high productivity and 0.1% for regions of intense upwelling. H. W. Menard and S. M. Smith [*J. Geophys. Res.* **71**, 4305 (1966)] showed that 7.5% of the ocean is shallower than 200 m, the classical definition of coastal waters. Because we found positive CH_3Br saturation anomalies in waters deeper than 200 m and have included less intense areas of upwelling in our estimate, we assigned 10% of the ocean to each of these regions.
22. S. Elliot and F. S. Rowland, *Geophys. Res. Lett.* **20**, 1043 (1993); W. Mabey and T. Mill, *J. Phys. Chem. Ref. Data* **7**, 383 (1978).
23. One residual standard deviation from a fit of atmospheric data to a locally weighted, statistical smoothing (LOESS) algorithm was 0.6 ppt [W. S. Cleveland, *J. Am. Stat. Assoc.* **74**, 829 (1979)].
24. E. Kossina, *Inst. Meereskunde Veröff. Geogr.-Naturwiss.* **9**, 70 (1921).
25. The partial atmospheric lifetime τ_0, with respect to oceanic loss is computed from

$$\frac{1}{\tau_0} = \frac{AK_w}{HM}\left(\frac{zk_s + \sqrt{k_zD_z}}{zk_s + K_w + \sqrt{k_zD_z}}\right) y^{-1} \quad (4)$$

with the area of the ocean $A = 361 \times 10^{12}$ m^2, the mean depth of the mixed surface water layer $z = 75$ m [see Y.-H. Li, T.-H. Peng, W. S. Broecker, H. G. Östlund, *Tellus B* **36**, 212 (1984)], the reciprocal solubility H for each oceanic regime (Table 2), the mass of the atmosphere $M = 1.77 \times 10^{20}$ mol, the air-sea exchange coefficient K_w (Table 2), and the in situ degradation rate k_s (*1*). The term for downward transport $\sqrt{k_zD_z}$ is calculated from an in-situ degradation rate k_z at an estimated thermocline temperture and the diffusivity D_z given by Li *et al.*
26. *Global Ozone Research and Monitoring Project (WMO Rep. 25*, World Meteorological Organization, Geneva, 1991). Mellouki *et al.* (*12*) included stratospheric losses in their estimate, whereas Zhang *et al.* (*13*) did not. We used a stratospheric lifetime of 50 years from the WMO report to adjust the number of Zhang *et al.*
27. J. M. Lobert *et al.*, unpublished results from *Polarstein* cruise ANT XII-1, October to November 1994.
28. R. Wanninkhof, *J. Geophys. Res.* **97C**, 7373 (1992).
29. This study was funded by the Methyl Bromide Global Coalition and the Atmospheric Chemistry Project of NOAA's Climate and Global Change Research Program. We thank M. R. Nowick for electrical expertise, E. Saltzman for critical review, the NOAA–Pacific Marine Environmental Laboratory group for their support, and the helpful crew of the *NOAA Ship Discoverer*.

27 July 1994; accepted 27 December 1994

Iceberg Discharges into the North Atlantic on Millennial Time Scales During the Last Glaciation

Gerard C. Bond and Rusty Lotti

High-resolution studies of North Atlantic deep sea cores demonstrate that prominent increases in iceberg calving recurred at intervals of 2000 to 3000 years, much more frequently than the 7000- to 10,000-year pacing of massive ice discharges associated with Heinrich events. The calving cycles correlate with warm-cold oscillations, called Dansgaard-Oeschger events, in Greenland ice cores. Each cycle records synchronous discharges of ice from different sources, and the cycles are decoupled from sea-surface temperatures. These findings point to a mechanism operating within the atmosphere that caused rapid oscillations in air temperatures above Greenland and in calving from more than one ice sheet.

The pioneering studies by Ruddiman and his colleagues of the North Atlantic's glacial record demonstrated that the amounts of drifting glacial ice were closely tied to Milankovitch-forced growth and decay of Northern Hemisphere ice sheets (*1–3*). Subsequent work on North Atlantic sediment from the last glacial cycle revealed in addition a higher frequency of iceberg discharges, about every 7000 to 10,000 years, that have come to be known as Heinrich events (*4, 5*). A leading explanation for the Heinrich events is surging of ice in Hudson Strait (*6*). Glaciological models, however, do not readily explain two recent findings. One is that five of the six Heinrich events occurred at the culminations of progressive coolings and were followed precipitously by warmings to almost interglacial temperatures (*7*). The second is that the youngest Heinrich event was nearly synchronous with rapid disintegration of the Barents ice sheet (*8*). In this paper we report results from high-resolution analyses of deep sea cores that bear further on mechanisms for ice-rafting events in the North Atlantic.

One of these findings is the presence of ice-rafting cycles in the intervals between Heinrich events. We identified these cycles, defined by variations in lithic concentrations [see also (*9*)], in two cores, DSDP site 609 and VM23-81 (Figs. 1 and 2). The records from the two cores match well (Fig. 2). Because the cores are separated by nearly 5° of latitude and are in different depositional environments, the correlation is not an artifact of local ocean surface or sea floor processes. Including the Heinrich events, there are 13 ice-rafting cycles in the interval from 10,000 to 38,000 radiocarbon years ago, yielding an average cycle duration of between 2000 and 3000 years (Fig. 2).

The evidence of a 2000- to 3000-year ice-rafting cycle in the North Atlantic is an intriguing result for it recalls the spacing of the Dansgaard-Oeschger temperature cycles (*10*), so convincingly documented by the measurements of $\delta^{18}O$ in ice from the recent drilling at Summit, Greenland (*11*). To investigate this relation further, we compared the $\delta^{18}O$ record in the GRIP ice core with lithic cycles in VM23-81 (Fig. 3). We first pinned the two records at the peak Younger Dryas cooling and then stretched the deep sea record until H4 matched the equivalent level in the ice identified by Bond and others (*7*). Below H4 the deep sea record was clipped and stretched again until the oldest peak in both records matched. Although the correlation was achieved with fewer clippings and stretchings than in (*7*), it is essentially the same. Between the Younger Dryas and H2, GRIP and GISP2 ages (*11, 12*) agree, within error, with ^{14}C to calendar age conversions (*13*). In addition, a sample of *Acropora palmata* from Barbados has a ^{14}C age of ~27,000 years ago and a U/Th age of 30,500 years ago (*13*), corroborating the GISP2 chronology we infer for the marine record (Fig. 3).

Our correlation demonstrates that all but one Dansgaard-Oeschger cycle corresponds to a lithic peak in the marine record (Fig. 3), indicating a close link between the shifts in air temperatures above Greenland and the ice-rafting cycles. Lithic peaks a, b, and c (Fig. 3), however, occur within the puzzling interval that lacks Dansgaard-

Lamont-Doherty Earth Observatory of Columbia University, Palisades, NY 10964, USA.